# VERIFICATION OF A 3D-CFD MODEL OF AN OLDHAM RING SCROLL EXPANDER

Saverio Randi[1]*, Nicola Casari[1], Ettore Fadiga[1], Alessio Suman[1], Michele Pinelli[1], Eckhard A. Groll[2], Davide Ziviani[2], Bryce Shaffer[3]

[1]Department of Engineering, University of Ferrara,
Via Saragat, 1 – 44122 Ferrara ITALY
saverio.randi@unife.it

[2]Ray W. Herrick Laboratories, Purdue University,
177 S. Russell St., West Lafayette, IN 47907-2099, USA

[3]Air Squared Inc.,
510 Burbank Street, Broomfield, CO, 80020, USA

* Corresponding Author

## ABSTRACT

Computational Fluid Dynamics (CFD) studies of volumetric expanders, such as scroll and rotary machines, are becoming more and more widespread due to the interest in these type of devices by Organic Rankine Cycle (ORC) systems manufacturers and because of the increasing available computational power, which makes these approaches more affordable than in past years and capable to provide useful information regarding transient phenomena. Scroll expanders are of particular interest for low-power output ORCs due to their cost-effectiveness. Most of scroll expanders rely on an Oldham coupling to maintain the orbiting motion of one of the wraps. The orbiting motion may lead to a non-uniform flow profile at the outlet of the discharge port, leading to vibrations of the machine due to gas pulsations.

In this paper, a CFD analysis of an open-drive scroll expander is carried out. The geometry of the expander is used to set up a transient 3D simulation by utilizing CONVERGE software. A Cartesian grid is generated and the scroll surface is mapped on this mesh. By utilizing this approach, the complex motion of the machine can be simulated, and the clearances can be discretized by employing an adaptive mesh refinement (AMR) technique, which guarantees a shorter computational time in comparison to the Overset method. The flow field is solved in both radial and axial gaps, while the motion of both the moving wrap and the Oldham ring is imposed by means of a user-defined function. The working fluid is R245fa and its properties have been imported from a thermodynamic database. Results have shown how CFD simulations were able to catch refrigerant behavior inside the machine, while the estimation of refrigerant mass flow was greatly affected by the absence of lubricant modeling, fluid which can be found, on the other hand, in the actual expander.

## 1. INTRODUCTION

Due to increasing concerns on Green-House emissions associated with primary energy production, Organic Rankine Cycle (ORC) systems are regarded as a viable technology to exploit medium to low-grade waste heat. ORCs are utilized to produce electrical power in both stationary and mobile applications. Although ORC for mobile applications are still at the development stage, as reported by Lion *et al.*(2017), and mainly focused on energy recovery from trucks because of their impact on $CO_2$ emissions (Guillaume *et al.*, 2017), stationary ORC systems are considered a mature technology with more than 350 MWe of installed capacity worldwide (Tartière and Astolfi, 2017). Several studies focusing on this type of applications have been published in the last decades, *e.g.* Mago and Luck (2013)

and Dong *et al.* (2011), but those regarding small and micro scale systems (below 10 kWe) are far scarcer. In such low power range, the use of dynamic machines as the expander is not favorable, as pointed out by Dong *et al.* (2011), because of the low energy conversion efficiency and high cost-effectiveness ratio. As a result, volumetric machines are more suitable for this type of applications. Since commercially available volumetric expanders are limited, it is common practice to reverse the operation of refrigeration compressors. For example, Woodland *et al.* (2012) modified an automotive scroll compressor to operate as an expander for a cycle using R134a as working fluid. They achieved an expander overall isentropic efficiency close to 75% with a filling factor close to unity. Ziviani *et al.* (2016) used a single-screw expander to run tests with two different refrigerants, *i.e.* R245fa and SES36, and found a peak overall isentropic efficiency of approximately 65% when operating with SES36. Bianchi *et al.* (2019) tested a micro-ORC fitted with a radial, three-cylinder piston expander and obtained overall efficiencies values ranging from 38% to 42% under the considered operating conditions. Dumont *et al.* (2017) tested four positive displacement expanders on the same ORC system, namely two different scroll machines, a swashplate piston and a twin-screw device. They found that, for a given configuration and using R245fa as working fluid, scroll-type expanders showed the highest isentropic efficiency (81 % versus 53 % of screw and piston types).

In this work, results of CFD analyses of an Oldham ring scroll expander are showed. Transient simulations have been carried out by considering R245fa as the working fluid. The analysis of the flow field inside the machine has also been conducted to assess flow losses. As pointed out by Suman *et al.* (2017) and Morini *et al.* (2015), one of the difficulties of running a time-dependent simulation of a scroll machine is the modeling of the orbiting motion of the moving wrap. More specifically, the variable radial gap width during machine operation decreases the mesh quality. In addition, the motion of the Oldham ring has been taken into account, because it is likely to influence the nearby flow. To author's knowledge, no research papers on CFD analyses of scroll machines including the Oldham rings have ever been published. For instance, Song *et al.* (2015) presented a comprehensive 3D CFD study of a scroll expander, but the presence of the orbiting mechanism has not been taken into consideration. Thus, a robust and sufficiently accurate approach which guarantees convergence of the solution has been adopted, given the 3D scroll geometry.

## 2. NUMERICAL MODEL

The original 3D scroll expander geometry has been simplified in order to execute the CFD study. In particular, all the elements such as screws and bolts were removed, along with gaskets and their seats. The resulting geometry is showed in Figure 1. On the left, a cut section of the machine in which the Oldham ring and the moving wrap are visible it is showed, while on the right a global view of the expander is presented. The machine analyzed in this work is characterized by flank and axial gaps with a minimum width of 50 µm. After this step, geometry was imported into the simulation software. At first, the same tool utilized by Suman *et al.* (2017) was intended to be used, due to the experience gained in modeling the spiral motion with the overset mesh technique. But when this model was applied at the current geometry, the total number of elements which composed the computational mesh was too high to let the simulation run up to convergence in a reasonable time. Thus, it has been chosen CONVERGE from Convergent Science because of its ability in simulating moving bodies without an excessive computational effort. In this software, to model the movement of the moving spiral no overset method is used. Instead, cells of the cartesian, numerical grid are cut using the given scroll geometry and, to take into account the narrow gaps in the geometry, the adaptive mesh refinement (AMR) algorithm has been used. This approach automatically refines computational grid only in those parts of the domain in which the gradient of a variable, such as velocity or temperature, is greater than a user-defined value.

For a variable-with-time domain such as the one showed in this work this means that, given a certain condition on the velocity field, the software will automatically refine mesh in several zones, including inlet and outlet ports. Another important aspect of this approach regards the condition which triggers the coarsening of the previously refined cells when the above criterion is no more met, namely when variable value is below one fifth of the user-defined value. This mesh refinement is done at runtime, reducing set-up time with respect to the software used in the previous cited work. Furthermore, in that case during simulation set-up mesh had to be manually refined also in those zones in which the overset

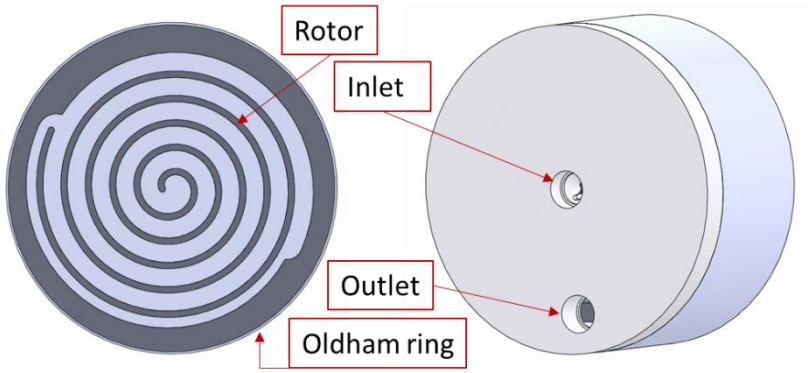


**Figure 1:** Simplified 3D scroll geometry

and background grids overlapped (these two types of grids are not available in CONVERGE), increasing the number of mesh elements. Due to the reduced computational effort, in the present study it has been possible to model also the movement of the Oldham ring, since its motion it is supposed to influence flow field at the outlet of the machine. In fact, the discharge port is placed directly in front of the ring, as shown in Figure 2. In order to allow these components to move, it is necessary to write a user defined function in which velocity, phase and orbiting radius of these components are taken into account.

### 2.1 Boundary conditions

The numerical model was set up as follows: an INFLOW boundary condition was placed at the inlet of the machine (which is placed in the middle of the housing, with 2400 kPa as inlet pressure and 523.15 K for the temperature), while a pressure of 250 kPa and temperature of 440.15 K were imposed at the OUTFLOW boundary. In this case, all the surfaces of the domain were considered as adiabatic walls. Velocity of the moving spiral was taken equals to 3600 rpm and the translation velocity of the Oldham ring was set up accordingly. This information is also reported in Table 1. Turbulence was modeled thanks to the RNG κ-ε model. About the wall treatment, a $y^+$ approach with standard wall function has been used, since dimensions of mesh elements have been chosen not to resolve the viscous sublayer. The base size of the computational cells was imposed to be equal to 1 mm in each dimension. However, by applying the AMR method, the number of elements of the mesh was not constant, but it varied from one to three millions, with the maximum admissible number of cells being fixed to five millions. Simulations were run using air at first and, then, R245fa as the working fluid. Air was initially adopted to test the simulation set-up without the numerical complexity of having a refrigerant as working fluid. The refrigerant was modeled as a real gas, but its properties have been determined by interpolating values reported in a look-up table. In particular, gas properties such as density, specific enthalpy, specific heat at constant pressure and volume, and many others were retrieved from the open-source CoolProp (Bell *et al.*, 2014) library and the simulation software was able to read the extracted values.
The CFD analyses have been carried out with a variable time-step as a function of the CFL (Courant-Friedrichs-Levy) number and the moving surfaces characteristics. Time-step values were free to fluctuate in the interval from $10^{-8}$ s to $10^{-5}$ s, while the maximum value for the CFL number has been set equal to 2.0 in order to guarantee the convergence of the simulation. With respect to the time-step limitation due to moving boundaries, the software takes into account (for a given moving surface) cell size and speed, as well as the value of a user-defined multiplier which, in this case, has been fixed to 0.5. The second order MUSCL (Monotonic Upstream-Centered Scheme for Conservation Laws) scheme has been used for the spatial discretization of the convective term of transport equations.

**Table 1:** Boundary conditions and geometric characteristics

| | | | |
|---|---|---|---|
| Inlet pressure [kPa] | 2400 | Inlet temperature [K] | 523.15 |
| Outlet pressure [kPa] | 250 | Outlet temperature [K] | 440.15 |
| Rotational speed [rpm] | 3600 | Gaps width [μm] | 50 |
| Suction volume [$m^3$] | 4.56e-6 | Nominal mass flow rate [kg/s] | 0.0275 |

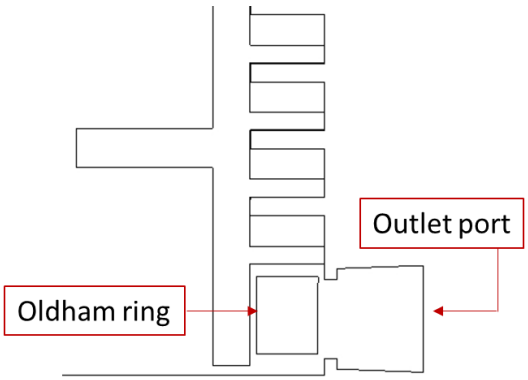


**Figure 2:** Detail of the outlet port

## 3. RESULTS

In order to analyze the behavior of the expander, the mass flow rate, the velocity profiles within the gaps, and the pressure variations within the chambers are analyzed. In order to assess the volumetric performance of a positive displacement expander, it is useful to introduce the filling factor, FF, as defined by Zanelli and Favrat (1994):

$$FF = \frac{\dot{m}_{suc}}{N \cdot V_{suc} \cdot \rho_{suc}} \tag{1}$$

where $\dot{m}_{suc}$ is the mass flow rate of refrigerant at the inlet of the machine, $N$ is the rotational speed, $V_{suc}$ is the suction volume and $\rho_{suc}$ the density of fluid at the inlet. In Figure 3, the instantaneous variations of the mass flow rate in and out the expander are reported as a function of spiral revolutions. In particular, fifteen revolutions are plotted. It can be noted how the flow rate is not constant during time, but it varies according to the motion of the moving spiral, for both the inlet and outlet ports of the machine. By calculating the filling factor with equation (1), a value of 2.58 is obtained. This value is lower than the one obtained when running the machine with air, but it is still higher than the experimental one (1.22, from manufacturer's data). This because the increase in fluid density at the outlet is almost compensated by the increase in mass flow. This behavior can be explained by the fact that in the actual expander, 5 % by mass of oil is added to the refrigerant, thus giving a sealing effect in the gaps. Since, in the current work, oil has not been modeled, this phenomenon has not been taken into account, leading to the presented result. To quantify these leakages, one can consider the expression for the filling factor written above. The theoretical mass flow at the inlet of the expander (denominator of equation 1) is equal to 0.0225 kg/s. This means that, for our case where the computed mass flow at the inlet is 0.0580 kg/s, the leakages are the difference between these values, thus they are equal to 0.0355 kg/s. To better check this result, a steady simulation with the same minimum values for radial and axial gaps of the unsteady one was run, giving a value of 0.034 kg/s.
Another reason for these values of the calculated leakages is represented by the fact that, in the real machine, gaskets fitted in both the fixed and moving spirals limit refrigerant flow across axial gaps, while in the model these parts has been omitted, as stated in Section 2. A way to take into account this phenomenon, as well as the absence of oil modeling, is to artificially decrease the value of gaps height in the numerical model.

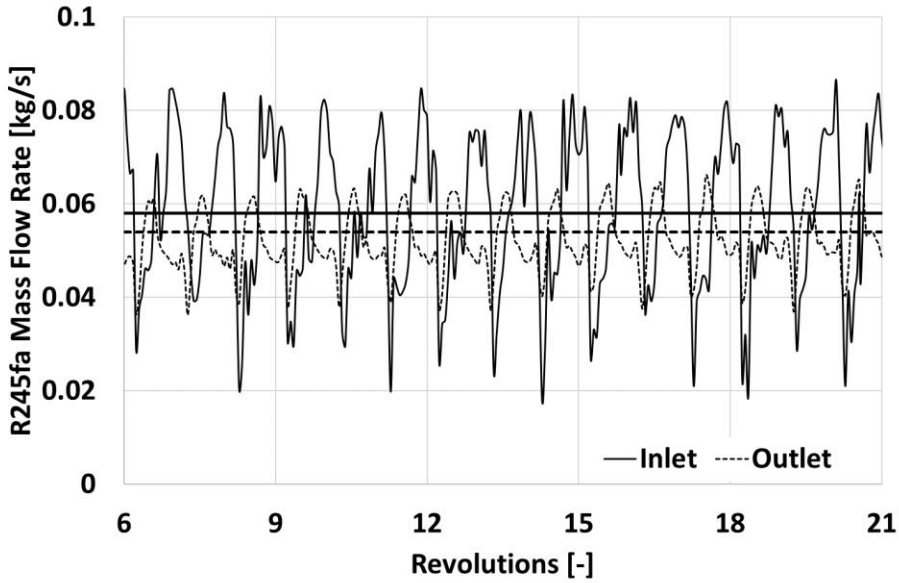


**Figure 3:** R245fa mass flow rate at the inlet (solid line) and outlet (dashed line) of the machine; straight lines represent mean values

In Figure 4, the pressure variation inside the scroll during a revolution is showed. The obtained pressure evolution is typical for such type of machines, with pressure gradually decreasing from the inlet port to the outlet one, with quite an even pressure distribution in the chambers around the suction port. It is also interesting to look at pressure traces at the inlet and outlet sections of the machine, to confirm what has been written at the beginning of Section 3 about flow rate pulsations. As shown in Figure 5, the pressure fluctuations are present at both ports, but at the outlet these are more pronounced than at the intake of the scroll, with peak values around 2 % of the nominal pressure (*i.e.* 250 kPa). In Figure 6, the flow pattern at the inlet and outlet sections of the machine are reported. In particular, at the discharge port, some recirculation occurs. To better analyze this phenomenon, a longitudinal section on the outlet and inlet ports has been extracted, Figure 7. From this picture, it is clearly visible recirculation at the outlet port: axial component of velocity should be negative on all the surface (since positive direction of z axis enters the screen), while some entering flow is always present for each instant of the simulation. It should be noted that Figure 6 and Figure 7 refer to a physical time of 0.174 s, but the same reasoning can be applied throughout many of the time steps simulated up to that point. This recirculation phenomena can be explained by the fact that, during its motion, the Oldham ring constantly occludes a certain portion of the outlet port thus, when the ring is moving to the upper position, the fluid previously entrapped behind this component is able to flow towards a lower pressure region. Because of the shape of the ring and of its motion, flow is pushed upward and thus recirculates.

In Figure 8, velocity peaks are present in both radial and axial gaps. This happens because clearances act as nozzles and the highest velocity is reached in the throat section, *i.e.* minimum gap height.

Results obtained from the numerical simulations suggest that lubricant modeling is an important aspect to consider, but it requires a great computational effort, because of the solution of mass, momentum and energy equations for both refrigerant and lubricant phases, with an Euler-Euler approach. To overcome these computational issues, the VOF method can be employed, where total mass, momentum, and energy transport equations are solved, along with the void fraction equation, which represents the fraction of cell volume that does not contain liquid. Anyway, in order to avoid excessive modeling error due to numerical diffusion, a fine mesh is required to accurately track the interface between the two phases. Thus, computational cost remains a critical aspect to care about.

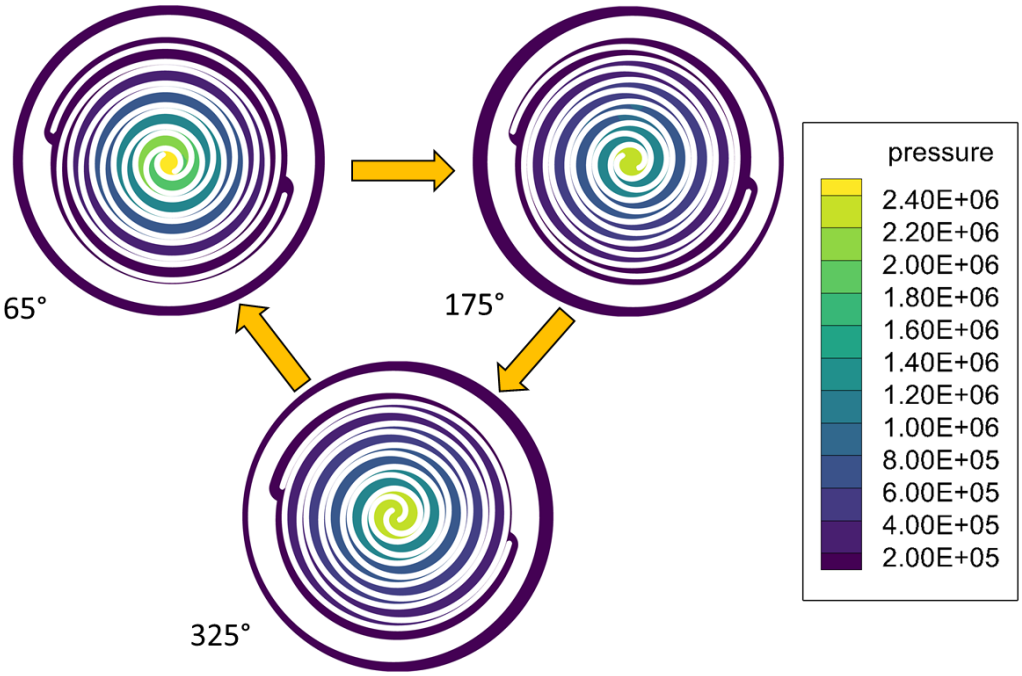


**Figure 4:** Static pressure field during one revolution of the moving scroll, values in [Pa]

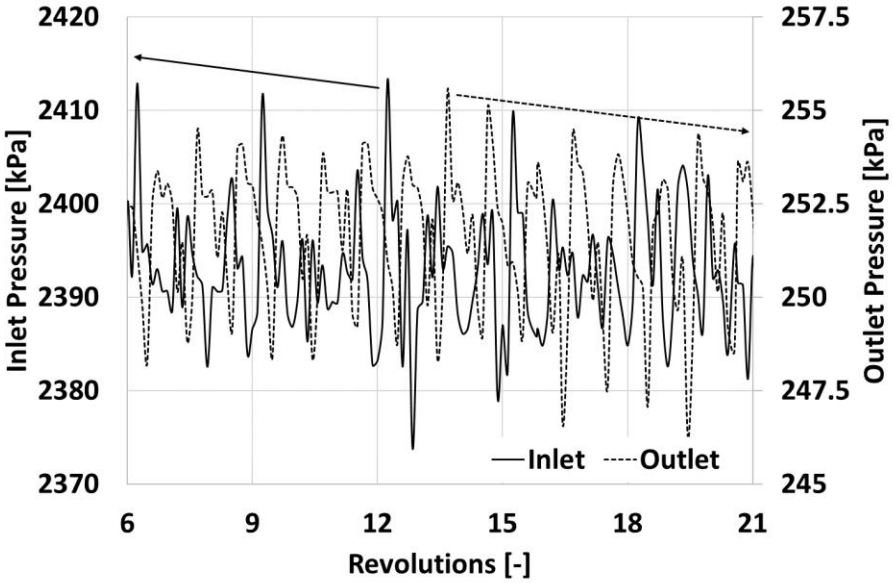


**Figure 5:** Pressure traces at inlet (solid line) and outlet (dashed line) ports

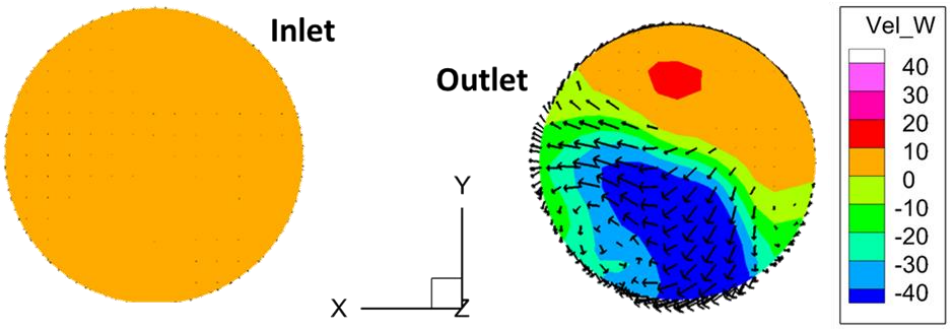


**Figure 6:** z-component of velocity at the inlet (left) and outlet (right) ports of the machine, front view, values in [m/s]

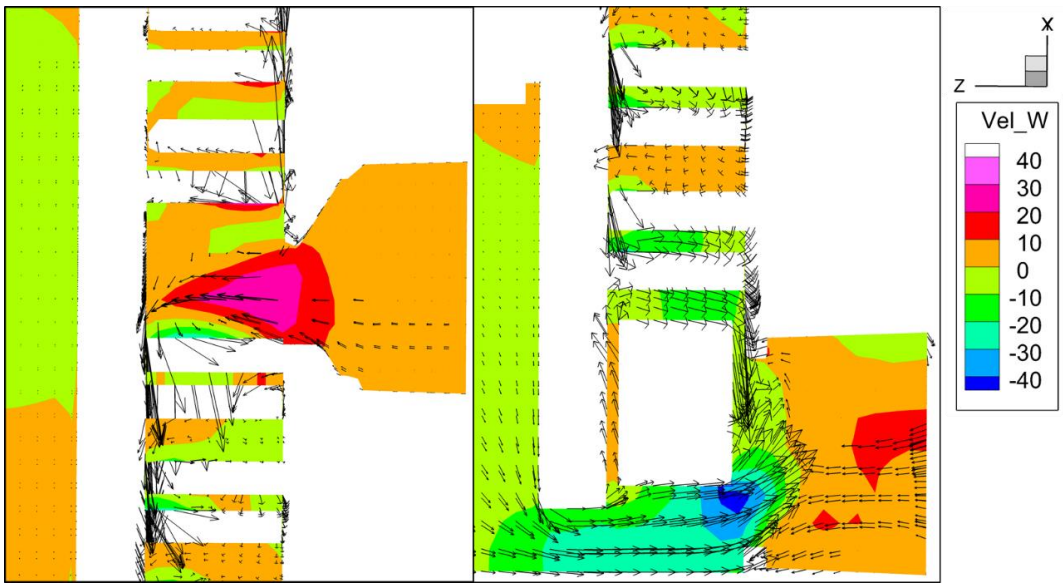


**Figure 7:** z-component of velocity at the inlet (left) and outlet (right) of the machine, values in [m/s]

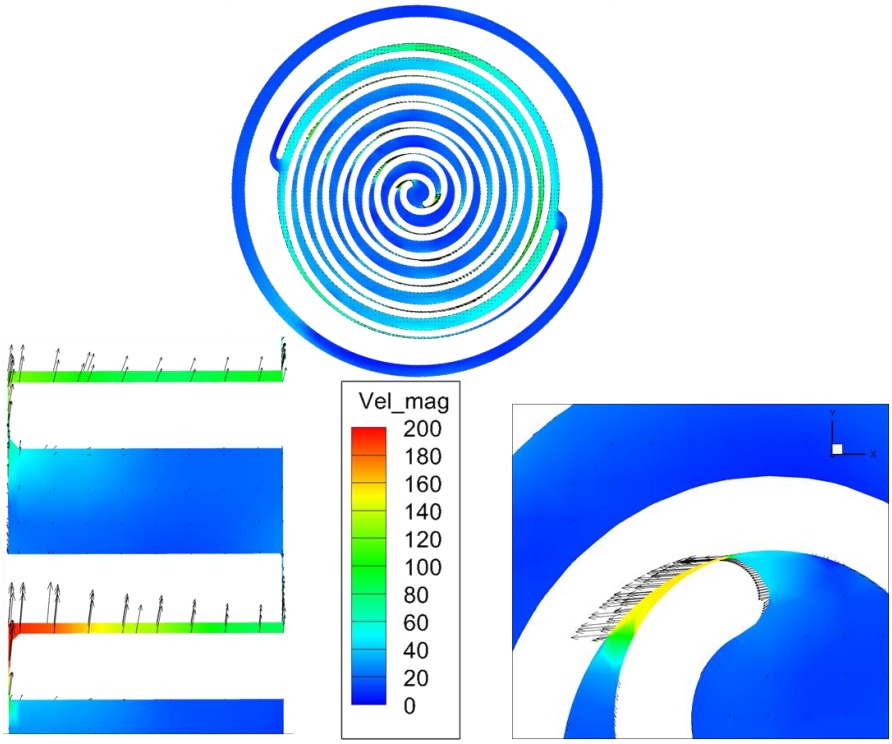


**Figure 8:** Velocity magnitude in the fluid domain, values in [m/s]

## 4.CONCLUSIONS

In this work, results of 3D CFD transient simulations of an Oldham ring scroll expander has been presented, with working fluids air and hydrofluorocarbon R245fa modeled as real gases. Motion of both the moving spiral and Oldham ring was imposed by means of an user-defined function. The numerical model has shown how the presence of the ring, placed in front of the exhaust port, can yield to recirculation of the fluid in that zone which, in turns, can reduce the available mass flow at the outlet of the machine. This effect is hidden by the presence of fluid leakages from radial and axial gaps, which lead to a higher mass flow through the simulated machine than the one in the actual expander.

## NOMENCLATURE

| | | |
|---|---|---|
| $y^+$ | dimensionless wall distance | (-) |
| FF | filling factor | (-) |
| $\dot{m}$ | mass flow | (kg/s) |
| N | rotational speed | (rps) |
| $V$ | volume | ($m^3$) |
| $\rho$ | density | ($kg/m^3$) |

**Subscript**

| | |
|---|---|
| in | inlet section |
| suc | suction |

## REFERENCES


Bell, I. H., Wronski, J., Quoilin, S., Lemort, V., 2014, Pure and Pseudo-pure Fluid Thermophysical Property Evaluation and the Open-Source Thermophysical Property Library CoolProp, *Ind Eng Chem Res*, vol. 53, n. 6: pp. 2498-2508.

Bianchi, M., Branchini, L., Casari, N., De Pascale, A., Melino, F., Ottaviano, S., Pinelli, M., Spina, P.R., Suman, A., 2019, Experimental analysis of a micro-ORC driven by piston expander for low-grade heat recovery, *Appl Therm Eng*, vol. 148: pp. 1278-1291

Convergent Science, 2018, Converge 2.4.24.

Dong, L., Liu, H., Riffat, S., 2011, Expanders for micro-CHP systems with organic Rankine cycle, *Appl Therm Eng*, vol. 29, n. 11-12: pp. 2119-2126.

Dumont, O., Dickes, R., Lemort, V., 2017, Experimental investigation of four volumetric expanders, *Energy Procedia*, vol. 129: pp. 859-866.

Guillaume, L., Legros, A., Dickes, R., Lemort, V., 2017, Thermo-economic optimization during preliminary design phase of organic Rankine cycle systems for waste heat recovery from exhaust and recirculated gases of heavy duty trucks, *Vehicle Thermal Management Systems conference*.

Lion, S., Michos, C. N., Vlaskos, I., Rouaud, C., Taccani, R., 2017, A review of waste heat recovery and Organic Rankine Cycles (ORC) in on-off highway vehichle Heavy Duty Diesel Engine applications, *Renew Sust Energ Rev*, vol. 79: pp. 691-708.

Mago, P.J., Luck, R., 2013, Evaluation of the potential use of a combined micro-turbine organic Rankine cycle for different geographic locations, *Appl Energ*, vol. 102: pp. 1324-1333.

Morini, M., Pavan, C., Pinelli, M., Romito, E., Suman, A., 2015, Analysis of a scroll machine for micro ORC applications by means of a RE/CFD methodology, *Appl Therm Eng*, vol. 80: pp. 132-140.

Song, P., Wei, M., Liu, Z., Zhao, B., 2015, Effects of suction port arrangements on a scroll expander for a small scale ORC system based on CFD approach, *Appl Energ*, n. 150: pp. 274-285.

Suman, A., Randi, S., Casari, N., Pinelli, M., Nespoli, L., 2017, Experimental and Numerical Characterization of an Oil-Free Scroll Expander, *Energy Procedia*, vol. 129: pp. 403-410.

Tartière, T., Astolfi, M., 2017, A World Overview of the Organic Rankine Cycle Market, *Energy Procedia*, vol. 129: pp. 2-9

Woodland, B.J., Braun, J.E., Groll, E.A., Horton, W.T., 2012, Experimental Testing of an Organic Rankine Cycle with Scroll-type Expander, *International Refrigeration and Air Conditioning Conference at Purdue.*

Zanelli, R., Favrat, D., 1994, Experimental Investigation of a Hermetic Scroll Expander-Generator, *International Compressor Engineering Conference*.

Ziviani, D., Gusev, S., Lecompte, S., Groll, E.A., Braun, J.E., Horton, W.T., van der Broek, M., De Paepe, M., 2016, Characterizing the performance of a single-screw expander in a small-scale orgnaic Rankine cycle for waste heat recovery, *Appl Energ*, n. 181: pp. 155-170.